



# The viscosity of pāhoehoe lava: *In situ* syn-eruptive measurements from Kilauea, Hawaii

Magdalena Oryaëlle Chevrel<sup>a,\*</sup>, Andrew J.L. Harris<sup>a</sup>, Mike R. James<sup>b</sup>, Laura Calabrò<sup>a</sup>, Lucia Gurioli<sup>a</sup>, Harry Pinkerton<sup>b</sup>

<sup>a</sup> Université Clermont Auvergne, CNRS, IRD, OPGC, Laboratoire Magmas et Volcans, F-63000 Clermont-Ferrand, France

<sup>b</sup> Lancaster Environment Centre, Lancaster University, Lancaster LA1 4YQ, United Kingdom

## ARTICLE INFO

### Article history:

Received 1 December 2017

Received in revised form 13 April 2018

Accepted 16 April 2018

Available online xxxx

Editor: T.A. Mather

### Keywords:

lava

rheology

rotational viscometer

bubbles

crystals

basalt

## ABSTRACT

Viscosity is one of the most important physical properties controlling lava flow dynamics. Usually, viscosity is measured in the laboratory where key parameters can be controlled but can never reproduce the natural environment and original state of the lava in terms of crystal and bubble contents, dissolved volatiles, and oxygen fugacity. The most promising approach for quantifying the rheology of molten lava in its natural state is therefore to carry out direct field measurements by inserting a viscometer into the lava while it is flowing. Such *in-situ* syn-eruptive viscosity measurements are notoriously difficult to perform due to the lack of appropriate instrumentation and the difficulty of working on or near an active lava flow. In the field, rotational viscometer measurements are of particular value as they have the potential to measure the properties of the flow interior rather than an integration of the viscosity of the viscoelastic crust + flow interior. To our knowledge only one field rotational viscometer is available, but logistical constraints have meant that it has not been used for 20 yr. Here, we describe new viscosity measurements made using the refurbished version of this custom-built rotational viscometer, as performed on active pāhoehoe lobes from the 61G lava flow of Kilauea's Pu'u 'Ō'ō eruption in 2016. We successfully measured a viscosity of  $\sim 380$  Pa s at strain-rates between 1.6 and 5 s<sup>-1</sup> and at 1144 °C. Additionally, synchronous lava sampling allowed us to provide detailed textural and chemical characterization of quenched samples. Application of current physico-chemical models based on this characterization ( $16 \pm 4$  vol.% crystals;  $50 \pm 6$  vol.% vesicles), gave viscosity estimates that were approximately compatible with the measured values, highlighting the sensitivity of model-based viscosity estimates on the effect of deformable bubbles. Our measurements also agree on the range of viscosities in comparison to previous field experiments on Hawaiian lavas. Conversely, direct comparison with sub-liquidus rheological laboratory measurements on natural lavas was unsuccessful because recreating field conditions (in particular volatile and bubble content) is so far inaccessible in the laboratory. Our work shows the value of field rotational viscometry fully-integrated with sample characterization to quantify three-phase lava viscosity. Finally, this work suggests the need for the development of a more versatile instrument capable of recording precise measurements at low torque and low strain rate, and with synchronous temperature measurements.

© 2018 Elsevier B.V. All rights reserved.

## 1. Introduction

Understanding and describing the complexity of lava flow behavior is a major challenge and a long-term objective in modern volcanology. Modeling of lava flows leads to significant improvements in hazard assessment, as well as contributions to our understanding of volcanic activity and history on other planets.

Rheology, which is directly linked to the intrinsic chemical and physical properties of the magma (chemical composition, oxygen fugacity, volatile content, temperature, and shape and size of bubbles and crystals) is a key influence on the transport of magma from its source to the surface (e.g., Dingwell, 1996). As lava flows, cooling and degassing trigger crystal and bubble growth and interstitial melt differentiation, driving constant evolution of the chemical and physical properties (e.g., Crisp et al., 1994; Applegarth et al., 2013). This continuous transformation leads to variations in rheological properties (viscosity, yield strength, strain-rate dependency) which directly impact the dynamics of lava flow

\* Corresponding author.

E-mail address: oryaelle.chevrel@gmail.com (M.O. Chevrel).

emplacement (e.g., Pinkerton and Norton, 1995; Harris and Rowland, 2001).

Several lava flow emplacement models exist in the literature (see Cordonnier et al., 2015 for comparison between the different models). Most of these models require parameterization of the lava physical properties (such as viscosity) and of the eruption conditions (such as eruption temperature or effusion rate), all of which are challenging to measure. Lava rheology can be determined using various methods. Following the pioneering study of Nichols (1939), lava rheological parameters can be estimated from flow velocity, underlying slope and channel dimensions assuming Newtonian or Bingham rheology. The advantage of this method is that channel velocity is a parameter that can be measured at any type of flow and provides the flow-scale ‘bulk rheology’ (e.g., Moore, 1987; James et al., 2007). However, this method cannot quantify the heterogeneity of rheological properties within and across a flow.

Another approach is to perform laboratory measurements using re-melted natural samples at super- and sub-liquidus conditions. Recent examples include Ishibashi (2009), Vona et al. (2011), Vetere et al. (2013), Chevrel et al. (2015), Sehlke et al. (2014), and Kolzenburg et al. (2016). These measurements are usually performed using a concentric cylinder apparatus, and the full rheological curve may be constructed for a given crystallinity and temperature. Recent experiments have explored the effect of cooling rate on crystallinity and the rheological response of the lava (Kolzenburg et al., 2016, 2017). Laboratory measurements have the advantage that they are made in an environment that allows key parameters to be controlled and precise rheological measurements to be made. However, they are unable to replicate the range of crystal and bubble contents, dissolved volatiles, and oxygen fugacity of natural lavas.

When laboratory experiments cannot be carried out, or when an active flow has not been observed, a common practice is to estimate viscosity from a “petrologic” approach. This involves applying empirical physico-chemical models based on previous laboratory experiments to estimate viscosity from groundmass chemical composition and crystal content (e.g., Pinkerton and Stevenson, 1992). This approach is clearly the best long-term method of providing rheological data for modeling volcanic processes because, being based on sample texture characterization, it can be applicable to present, past or extraterrestrial deposits. The petrologic approach may be applied to quenched samples from an active flow, where the groundmass crystallization will evolve as a function of cooling through time and distance from the vent (e.g., Crisp et al., 1994; Riker et al., 2009). The effect of bubbles (term used when describing the molten lava) may also be taken into account from estimation of the vesicle (term used when describing the rock) content, which may also vary down flow (Robert et al., 2014). Another use of this method is to determine the viscosity from the crystallization sequence as calculated at thermodynamic equilibrium (e.g., Harris and Rowland, 2001; Riker et al., 2009; Chevrel et al., 2013). However, care must be taken when assuming thermodynamic equilibrium because lava flows are undercooled systems whose properties (crystallization and hence rheology) are cooling-rate dependent (Kolzenburg et al., 2016). During flow, lava does not reach the crystal/melt equilibrium and this disequilibrium leads to a delay in crystallization that must be accounted for when calculating lava viscosity down flow.

Currently, the only way to determine the complex rheological behavior of lava in its natural state is to measure it directly in the field by inserting a viscometer into the molten lava while it is flowing. Such *in-situ* viscosity measurements are notoriously challenging to perform due to the difficulty of approaching an active lava flow, and the lack of appropriate instrumentation. A small number of viscosity measurements have been made using either penetrometers (Einarsson, 1949; Gauthier, 1973;

Panov et al., 1988; Pinkerton and Sparks, 1978; Belousov and Belousova, 2018) or rotational viscometers (Shaw et al., 1968; Pinkerton et al., 1995b; Pinkerton, 1994). Among these studies, measurements performed using simple lava penetrometers (a metal rod pushed into the lava) produce results that are influenced by the outer viscoelastic layer. Measurements start as soon as the sensor is inserted into the lava so that the viscosity of the viscoelastic crust + flow interior is integrated. However, all rotational viscometers, and the custom-built penetrometer used by Pinkerton and Sparks (1978), have the potential to measure the properties of the flow interior because measurements start once the isothermal interior is reached. The viscous core of large ‘a’ā flows remains inaccessible for field viscometry, due to the problems of penetrating the overlying breccia layer. Low viscosity lava flows, such as pāhoehoe type and small channelized flows are the only targets so far accessible by field viscometry.

To our knowledge, viscometers developed by the University of Lancaster in the 1980s and 1990s (Pinkerton, 1994; Pinkerton et al., 1995a, 1995b) are the only portable rotational viscometers to have been used *in situ* on active lava flows, with the last measurements performed more than 20 yr ago (Pinkerton, 1994; Pinkerton et al., 1995b). Since then no further work has been presented due to lack of suitable conditions and personnel (and funds) dedicated to the project. Conversely, over the past decades, extensive laboratory measurements on natural or analogue mixtures have greatly improved our understanding of the chemical control of the melt phase on viscosity (e.g., Giordano et al., 2008), as well as the rheology of two-phase mixture (e.g., Mader et al., 2013). As a result, although many physico-chemical based models now exist to estimate the rheology of magmas and lavas, no field measurements have been performed to test whether, and how, they can be applied to natural lava flows. Additional field validation is therefore required to provide confidence in the petrologic approach.

In this work, we restored the unique field rotational viscometer of Pinkerton et al. (1995b) and performed viscosity measurements on pāhoehoe lobes at Kilauea, Hawaii. The aims of this paper are to present this refurbished instrument and our new field measurements. Our viscometry results are described in detail, and complemented by textural and chemical analyses performed on quenched samples, which we use to implement, and compare with, a petrologic approach.

## 2. Methods

### 2.1. Viscometry

#### 2.1.1. Description of the field viscometer

We restored the rotational viscometer used by Pinkerton et al. (1995b) for field measurements (Fig. 1). This instrument consists of a 24-V DC variable speed Bosch drill that drives a vane, which is inserted into the lava. The vane geometry is unlike many laboratory instruments, where the immersed spindle is often a cylinder. Instead it was designed for field use to minimize disturbance of the fluid during immersion whilst minimizing slippage between the spindle and lava. The vane is attached to the rotating inner shaft which is protected with a fixed outer tube equipped by bearing assemblies (containing graphite rings to minimize friction). This helps to maintain alignment and low-friction rotation of the inner shaft (Fig. 1a), which is driven by the drill via a 15:1 reduction gearbox, a torque limiter (2 Nm), and a torque and rotation rate sensor (TORQSENSE E300 Rayleigh Wave Transducer from Sensor Technology Ltd). The sensor is linked to a stand-alone E302 interface/readout connected to a laptop via USB, and is a different version to the one in Pinkerton et al. (1995b). In 2016, the torque sensor and transducer were calibrated by Sensor Technology and

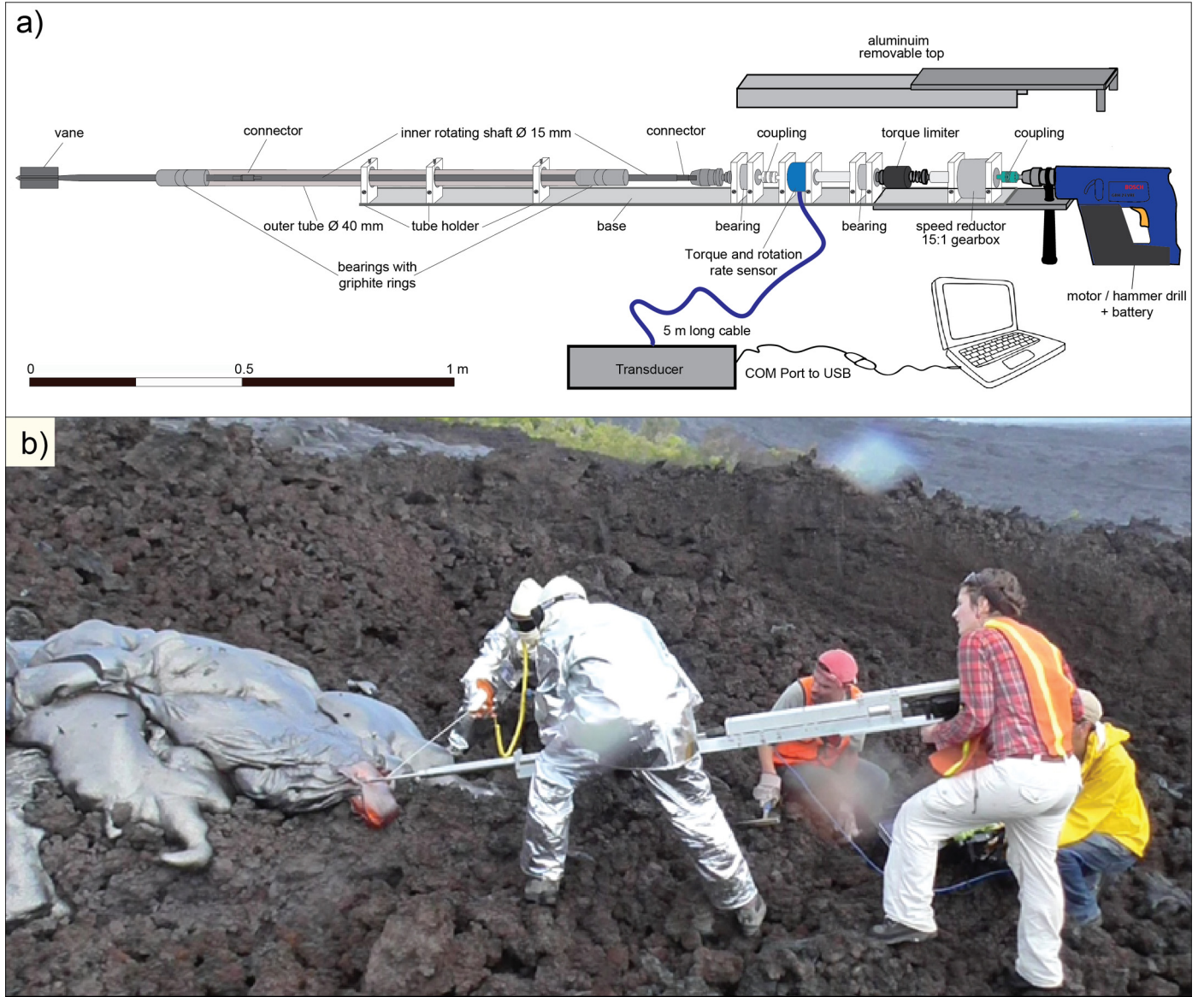


**Fig. 1.** a) Schematic of the viscometer. b) Field viscosity measurements (Run 1) of the 61G lava break out on November 23, 2016 (N19.349537, W155.048793). The two people most exposed to the hot lava are equipped with heat suits and goggles. One is holding the viscometer in position and the other is taking temperature measurements with an 80 cm long, K-type thermocouple with a 15 mm thick sheath.

small adjustments in communication were made so that the computer simultaneously recorded the rotation rate and torque every 0.05 s through the software provided (TORQVIEW2). At rest, we recorded a sensor sensitivity of  $\pm 0.02$  Nm. When a rotation was applied with the instrument mounted with the vane in air, an oscillation of  $\pm 0.05$  Nm was recorded, although efforts were made to reduce this by improving the alignment of the rotating rod between the motor and the vane. New shear vanes were made using the same type of high temperature-resistant stainless steel (BS 321 S20 or Z6CNT18.10) as used for the inner shaft and outer tube. Two vane sizes were employed, both composed of four paddles (2 mm thick) welded at  $90^\circ$  onto a 1 cm diameter rod, so that the vane diameter across the fins is 40 mm for the 60 mm-long vane (hereafter S60/20), and 50 mm for the 80 mm-long vane (hereafter S80/25). The total length of the assembled apparatus is 2.7 m, has a weight of about 15 kg, and can be dismantled into four pieces for transport.

### 2.1.2. Data processing to extract viscosity

The theory employed is that of wide-gap concentric cylinder viscometry. Here, the torque is converted into shear stress and rotational speed into strain-rate using the spindle geometry via the Couette theory for Newtonian or non-Newtonian fluids (Spera et al., 1988; Pinkerton and Norton, 1995; Stein and Spera, 1998; Vona et al., 2011). Material trapped between the paddles will move as the spindle rotates and therefore a virtual cylinder of sample material is used for the calculation. The shear stress is calculated via:

$$\tau = \frac{M}{2\pi h R_i^2} \quad (1)$$

where  $M$  is the torque recorded by the torque sensor,  $h$  is vane length and  $R_i$  is the equivalent radius of the rotating vane. Strain rate is obtained from the applied angular velocity via (Stein and Spera, 1998):



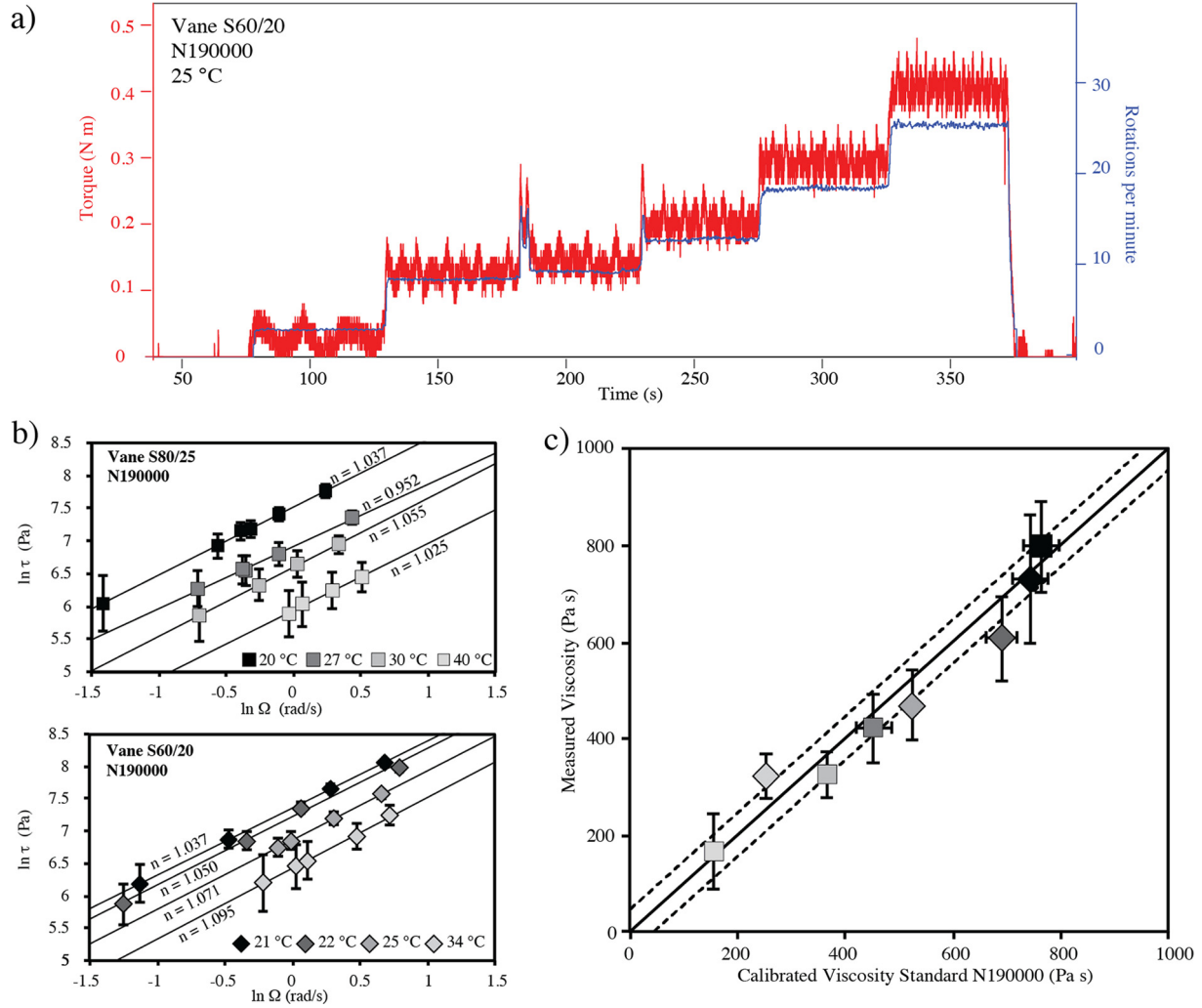


**Fig. 2.** Results of testing the rotational field viscometer in the laboratory, using the viscosity standard N190000 from Cannon Instrument Company® at various temperatures; a) Example of raw data acquired in the laboratory; b) Flow curves obtained using both vanes; c) measured viscosity versus theoretical values of the standard viscosity liquid calculated using the relationship obtained from certified values at the experimental temperature. Horizontal error bars represent the viscosity variation across the plastic container due to the temperature gradient (if not visible they are smaller than the symbol). Vertical error bars represent the range of estimated viscosity over the different strain rates and instrument accuracy. The solid line gives the 1:1 relationship and dashed lines delimit an interval of  $\pm 50$  Pa s. Squares are for measurements using the 80 mm long and 50 mm diameter shear vane (S80/25) and triangles are for measurements using the 60 mm long and 40 mm diameter shear vane (S60/20).

$$\dot{\gamma} = \frac{2\Omega}{n(1 - (\frac{R_i}{R_o})^{2/n})} \quad (2)$$

where  $\Omega$  is angular velocity (in rad/s),  $n$  is the flow index, and  $R_o$  is the radius of the outer cylinder. In the case of field measurements, the vane is effectively immersed into an unconstrained medium (i.e.,  $R_o$  approaches infinity). Now, following Barnes (1989; see supplement), the calculation of strain rate (for a range of 0.1 to 10  $\text{s}^{-1}$ ) can be reduced to:

$$\dot{\gamma} = \frac{2\Omega}{n} \quad (3)$$

When several angular speeds are applied,  $n$  is usually obtained by calculating the slope of the measured  $\ln(\tau)$  vs.  $\ln(\Omega)$  relation. The flow curves (i.e., the graph of strain rate versus shear stress) can then be established to determine the fluid's rheological model. This is Newtonian when viscosity is proportional to strain rate ( $n = 1$ ):

$$\eta = \frac{\tau}{\dot{\gamma}} \quad (4)$$

or non-Newtonian when viscosity varies with strain rate ( $n \neq 1$ ) as, for example, in a power law model:

$$\tau = K\dot{\gamma}^n \quad (5)$$

Here  $K$  is the flow consistency, which corresponds to viscosity at unit strain rate.

In practice, when measuring rheology, if one or only a few angular velocities are applied, the full flow curve cannot be reliably established so that  $n$  cannot be accurately determined. A common practice is therefore to calculate the apparent viscosity that is equivalent to the Newtonian viscosity. This can be determined at each applied strain rate by assuming  $n = 1$ .

### 2.1.3. Testing the field viscometer in the laboratory

The instrument was tested in the laboratory using the viscosity reference standard N190000 from Cannon Instrument Company®. This has been certified to be 33.06, 143.8, 523.3 and 843 Pa s at 60, 40, 25 and 20 °C, respectively. These certified values were used to define the exponential relationship:  $\eta = 3990.7e^{-0.081T}$  ( $R^2 = 0.99$ ), allowing us to estimate the viscosity of the N190000 standard at experimental temperatures. To perform the measurements, 1.5 L of N190000 viscosity standard were poured into a plastic container, which was 12 cm in diameter and 15 cm deep. Before each experiment, the fluid was placed overnight in an oven at the desired temperature to allow equilibration and removal of all air

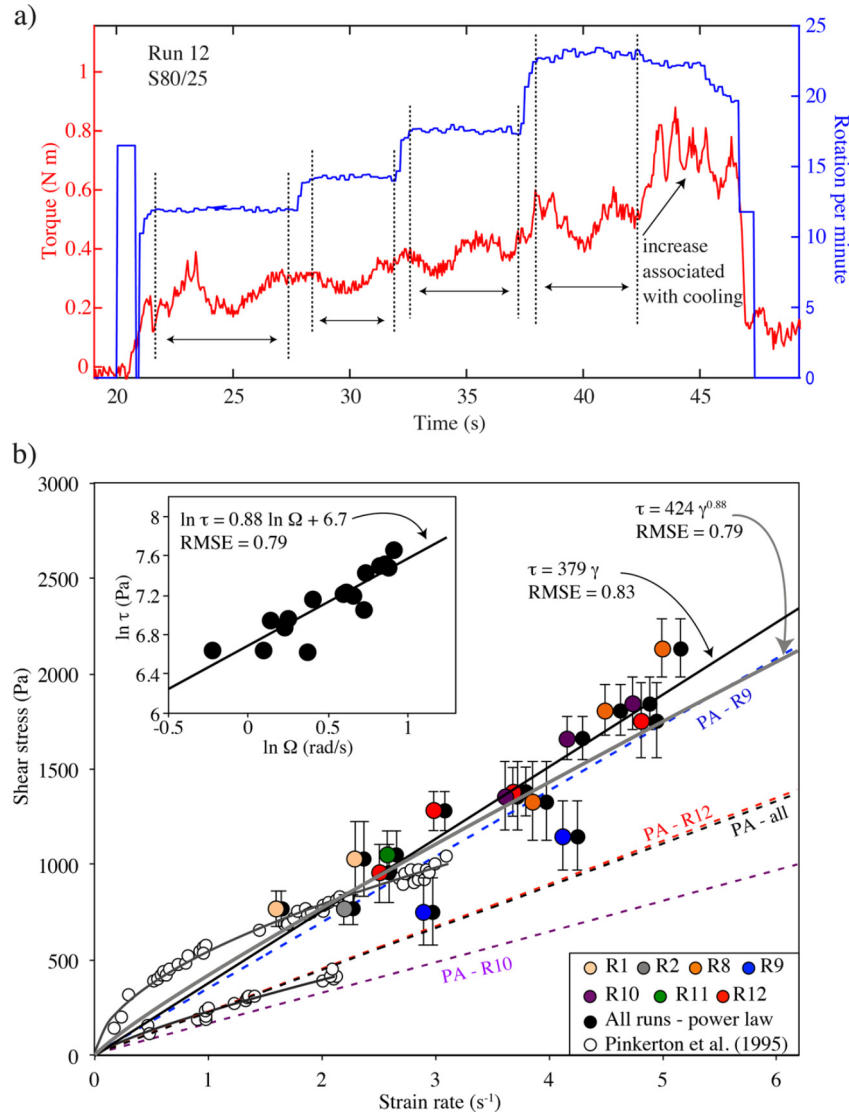


**Fig. 3.** *In-situ* measurements obtained at the 61G lava flow, on November 23, 2016 (N19.349537, W155.048793): a) Example of raw data acquired where horizontal double arrows show the range of constant speed over which torque was averaged; b) each data point is an average value over stable readings and error bars represent the fluctuation of the torque measurements (see supplement). Colored symbols are for individual runs treated as Newtonian, black symbols represent runs treated as having a power law rheology (see inset), and white symbols are the measurements from Pinkerton et al. (1995b) which are treated as a power law rheology. The grey curve represents the best power law fit and the black line is the linear Newtonian fit; the dashed lines represent the viscosity values as calculated from the petrologic approach (PA) using the chemical and textural characteristics averaged for all samples, and for samples quenched after viscosity measurements (R9, R10 and R12). (For interpretation of the colors in the figure(s), the reader is referred to the web version of this article.)

bubbles. Prior to each calibration, the container was removed from the oven and the temperature of the fluid measured using a K-type thermocouple located in the liquid beside the vane. Temperatures across the container varied by less than 2 °C and were constant near the vane during the experiment, with a maximum variation of  $\pm 0.6$  °C. The instrument was oriented at an angle of 45° and the container was inclined so that the vane was fully immersed into the liquid. Both vanes were tested at several temperatures between 20 and 40 °C and over rotation speeds of 2 to 20 rpm, resulting in strain rates adjacent to the vane of 0.6 to 5 s<sup>-1</sup> (calculated using Eq. (2)). Higher strain rates were not applied because of shear thinning effects that will bias the measurements (Cannon Instrument Company, personal communication, October 2016). The average torque was obtained over 8 to 60 s of stable reading at different strain rates at each temperature (Fig. 2 and supplement). The  $\ln(\tau)$  vs.  $\ln(\Omega)$  trends (Fig. 2b) had slopes of  $n = 1 \pm 0.09$  as expected for Newtonian behavior of the N190000 viscosity standard. Apparent deviation from Newtonian behavior was observed

when torque was less than 0.1 N m (equivalent to stresses of 318 and 663 Pa for vanes S80/25 and S60/20, respectively). This is attributed to limits in the torque transducer capability at low torque values, and therefore only higher torque measurements were considered. Viscosity was then calculated following wide gap theory (Eqs. (1), (2) and (4)) for Newtonian behavior. Less than 5% of error and less than 50 Pa s of deviation from the standard values was found (Fig. 2c).

#### 2.1.4. Operating the field viscometer in the field

To perform a measurement in the field, two people held the instrument (Fig. 1b). The operator closest to the lava inserted the vane into the active lobe and held it in position in the middle of the fluid core taking care not to ground the vane. The second person controlled the drill speed and monitored the data being collected on the computer. When the targeted lava lobe was surrounded by other hot surfaces, the computer would be monitored by a third person located a couple of meters away in cold air and

**Table 1**  
Field viscometry results.

Exp. number	Vane	Time (s)	Rotations per minute	Angular velocity (rad/s)	Torque (N m)	±	Shear stress <sup>a</sup> (Pa)	±	Strain rate <sup>b</sup> (s <sup>-1</sup> )	Viscosity <sup>c</sup> (Pa s)
Run 1	80/25	7	7.6	0.80	0.24	0.03	769	90	1.6	483
		7	11.0	1.15	0.32	0.05	1030	194	2.3	449
Run 2	80/25	23	10.5	1.10	0.24	0.02	767	79	2.2	349
Run 8	60/20	3	18.6	1.93	0.20	0.04	1332	204	3.9	345
		3	21.5	2.25	0.27	0.02	1810	135	4.5	403
		4	23.8	2.50	0.32	0.02	2132	154	5.0	427
Run 9	60/20	3	13.8	1.44	0.11	0.03	755	173	2.9	261
		7	19.7	2.06	0.17	0.03	1152	179	4.1	280
Run 10	60/20	6	17.2	1.80	0.20	0.03	1359	177	3.6	377
		4	19.9	2.08	0.25	0.02	1664	116	4.2	400
		4	22.6	2.37	0.28	0.02	1842	135	4.7	389
Run 11	60/20	6	12.3	1.29	0.16	0.04	1062	119	2.6	413
Run 12	80/25	6	11.9	1.25	0.30	0.05	955	153	2.5	382
		11	16.3	1.49	0.40	0.03	1284	104	3.0	430
		5	17.6	1.84	0.43	0.04	1380	128	3.7	375
		5	23.0	2.40	0.55	0.06	1756	200	4.8	366

<sup>a</sup> Calculated with Eq. (1).

<sup>b</sup> Calculated with Eq. (3) and  $n = 1$ .

<sup>c</sup> Calculated with Eq. (4).

who would direct operations. At the same time, temperature measurements were made with a K-type thermocouple (Fig. 1b). This was done only for the first measurement because, after this, the third person was needed to perform other measurements. Before insertion, the vane was pre-heated by being placed close to the lobe surface and exposed to the radiant heat. However, this pre-heating procedure did not last more than few seconds and could not always be performed because the active lobe cooled too rapidly so that an impenetrable outer crust formed, or because operators could not handle the radiant heat themselves. The instrument was then rapidly inserted into the hottest and most fluid part of the active lobe and the measurement started. As the lava advanced and its surface began to solidify, the instrument was slowly pulled backwards by the operator. Each measurement lasted less than one minute, mainly due to lava cooling around the rod to prevent rotation. Radiant heat was also a limiting factor for the operators, despite the use of heat protective suits and hoods. Although we aimed to reach a stable reading over 20 s (as in the laboratory), it was not always possible because the surface cooled too quickly and imprisoned the spindle. To record a range of strain rates, the angular velocity was manually increased (“up path”) and then decreased (“down path”) by changing the drill speed. However, practicalities meant that it was not always possible to cover the full up and down path ranges. To estimate the apparent viscosity, the torque recorded during constant drill speed over at least 3 to 23 s was then averaged and the standard deviation from the mean used for error bars (see example in Fig. 3a and raw data in supplement).

## 2.2. Lava sampling and textural analyses

Samples were collected after each viscosity measurement by quenching the lava attached to the vane in a water bucket. Another set of samples was collected using a stainless steel tube inserted into an active pāhoehoe lobe. The tube was inserted into the lobe front and withdrawn from the lava before quenching with water, effectively coring the tube. Additionally, one control sample was collected from a pāhoehoe lobe emplaced a few weeks earlier. Bulk rock major element analysis of one sample was carried out with Inductively Coupled Plasma – Atomic Emission Spectroscopy at the Laboratoire Magmas et Volcans (LMV, Université Clermont-Auvergne, France). Thin sections were made from all samples, and textural and chemical analyses were carried out at LVM. Olivine and glass chemical compositions were obtained from around 10–20 analyses for each thin section via the electron microprobe (CAMECA SX 100), operating at 15 kV and with a focused

beam of 15 nA for olivine and a 20  $\mu\text{m}$  defocused beam of 8 nA for glass. Total water content was determined from double polished samples by Fourier Transform Infrared Spectroscopy, using a Bruker Vertex 70 spectrometer coupled with a Hyperion microscope system, following the methods given in Mercier et al. (2010, see supplement). Crystallinity, vesicularity and vesicle size distribution were estimated from analyses of the thin sections through FOAMS following the methods described in Shea et al. (2010). For each thin section, high magnification images were acquired with scanning electron microscopy (SEM) in BSE (backscattered electron imaging mode) at  $\times 25$  magnification (six images in total), and  $\times 100$  (fifteen images in total). The smallest object measured was 10 pixels across (equivalent to 0.012 mm).

A mean value (averaged from two to four measurements) for the vesicle-free rock density (DRE density) was determined by powdering the rock and measuring the volumes of known masses using an Accupyc 1340 Helium Pycnometer. The bulk density of the samples was measured using a pycnometer (Micromeritics Geopyc 1360 envelope density analyzer). This instrument calculates the envelope density of the sample, which is the mass divided by its encompassing volume, where the encompassing volume includes pores and small cavities. The measurement technique consists of measuring the difference in the volume of a quasi-fluid medium (DryFlo™, composed of tiny, rigid spheres) with and without the sample embedded in the medium. Prior to immersion samples were wrapped with parafilm™ to preserve external irregularities but to avoid the medium entering the porous sample. The density-derived vesicularity was then calculated using the relationship given by Houghton and Wilson (1989).

## 3. Results

The targeted lava flow was the 61G flow of Kilauea’s Pu’u Ō’ō eruption (Hawaii) which had been active since May 2016. At the time of the field campaign, the lava was mainly flowing in tubes from the vent down to the ocean entry, but on November 23, 2016, we were able to deploy the instrument on several pāhoehoe lobes at N19.349537, W155.048793. These had broken out from the tube 7.2 km from the vent overnight. The lava flow field consisted exclusively of S-type pāhoehoe lava with a bubble-rich silvery surface. Each observed lobe was 10–30 cm thick upon emplacement and was active for about three to five minutes before stalling, inflating and erupting another lobe from its base. Core temperature was measured at 1144 °C with a K-Type thermocouple inserted to 5 to 8 cm into the lobe (Fig. 1b).



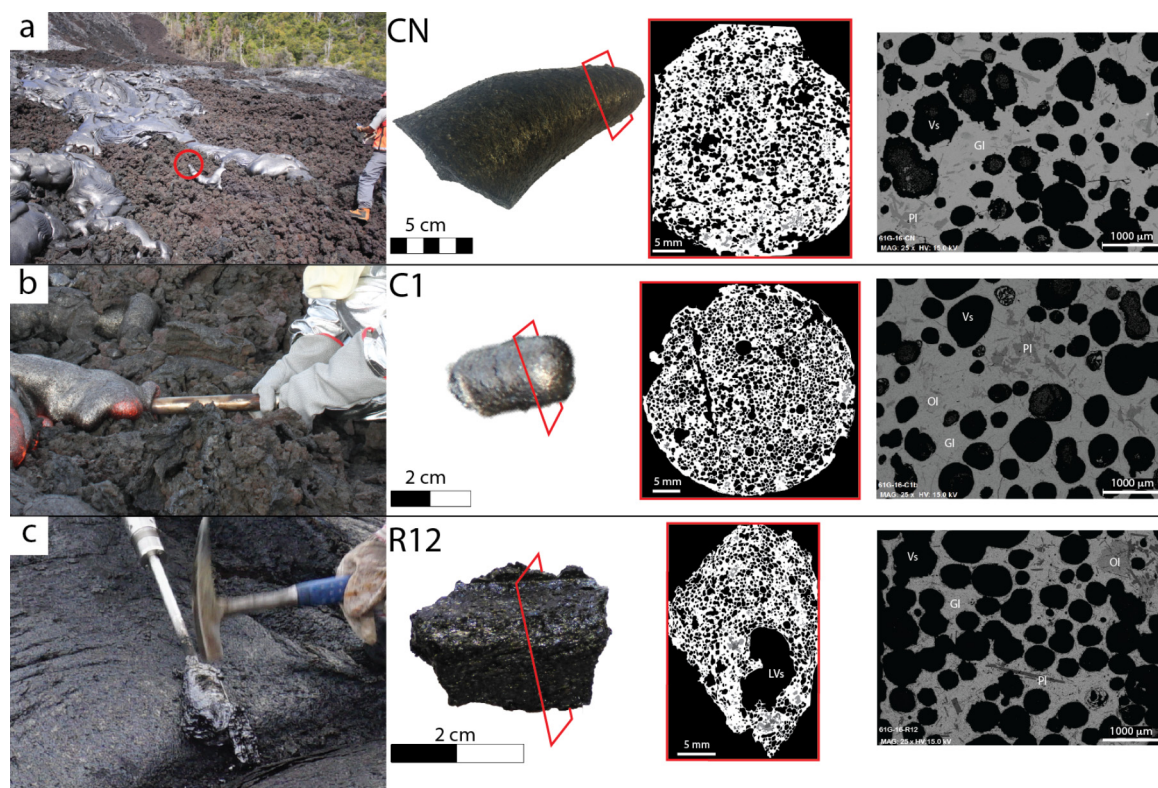


**Fig. 4.** Collected samples, from left to right field setting, hand sample, binary image of thin section scans (white is the glass, black are the vesicles and grey are the phenocrysts), SEM image at  $\times 25$  magnification: a) control sample (CN), collected on a breakout pāhoehoe lobe a few weeks old; b) example of a sample (C1) collected using a stainless steel tube inserted into the front of a pāhoehoe lobe and quenched rapidly in water, c) example of a sample (R12) collected from the lava attached to the vane after viscosity measurement and quenched in water. Red boxes indicate the thin section locations. Abbreviations are: Gl: Glass; Ol: Olivine; Pl: Plagioclase; Vs: Vesicles; LVs: Large vesicles formed during sampling (observed in quenched samples but absent from the control sample).

### 3.1. Viscometry

Viscosity measurements were successfully performed on seven distinct lobes. For each run, between one and four strain rates associated with stable torque readings could be collected before the spindle stopped rotating due to lobe cooling (the example of run 12 is given in Fig. 3a) or due to operator discomfort because of having to stand on an active surface or strong radiative heat. For four runs (R2, R9, R10, R11), data could also be collected during the down path but showed a marked hysteresis when compared with the up path, resulting in a higher apparent viscosity (see supplement). A similar viscosity increase was also recorded for some measurements within the up path phase (for example R2, R8, R9), which could be interpreted as representing shear thickening. However, shear thickening has not been observed in previous lava rheology measurements, so the effect is more likely to be due to rapid cooling of the lobe, or to the accumulation of cooled lava around the vane. Both would have significantly increased the effective diameter of the spindle. Considering data that were not affected by this phenomenon, rotation velocities ranged from 7.6 to 23.8 rpm, corresponding to strain rates between 1.6 and  $5 \text{ s}^{-1}$  at the vane. Torque was recorded between 0.11 and 0.55 N m, reflecting shear stresses of between 755 and 2132 Pa (Table 1). The apparent viscosity at each strain rate was determined to be between 261 and 483 Pa s. Unfortunately, the limited number of measurements possible at each lobe did not allow us to construct the full rheological flow curve with confidence. We also note that no yield strength was measured. Gathering all runs into a single plot (Fig. 3b) shows that the lava had a Newtonian viscosity (Eq. (4)) of 379 Pa s ( $R^2 = 0.83$ ). Treating the data as a power-law rheology (Eq. (5)) gave a flow index of 0.88 and a consistency of 424 Pa s ( $R^2 = 0.79$ ).

### 3.2. Sample chemical analyses and textural characterization

Bulk rock analysis revealed 50.8 wt.%  $\text{SiO}_2$  and a Mg# of 0.38 (Table 2), with a DRE density of  $2847 \text{ kg m}^{-3}$ . The interstitial glass chemical composition was identical and homogeneous in all samples and slightly more evolved than the bulk rock, with a water content of  $0.077 \pm 0.015 \text{ wt.}\%$  (Table 2). All samples had a porphyritic texture containing phenocrysts mainly of olivine and rarely of plagioclase, along with microlites ( $< 0.1 \text{ mm}$ ) of olivine and plagioclase, as well as minor pyroxenes and minor oxides (usually as inclusions in olivine phenocrysts). These were embedded within a glassy matrix (Fig. 4). Olivine crystals had euhedral and sub-euhedral shapes and in some samples (CN, C1a and R9), they were organized in glomerocrysts with plagioclase (Fig. 4c). Plagioclase occurs mostly as microlites (in some samples all plagioclase were as microlites) and pyroxene was the least abundant phase and occurred only as microlites. The aspect ratio (length vs. width) of the mafic minerals was 1.8 and 3.1 for plagioclase. The vesicle-free crystal fraction (phenocrysts + microlites) varied from 0.12 to 0.21 (Table 3). Overall, the similarity in crystal shape and content between the control sample and the quenched samples indicated that our sampling technique did not affect the texture of the lava. Therefore, the quenched samples could be used to estimate the effect of crystals on viscosity.

In terms of vesicularity, the quenched samples showed some differences with the control sample. The control sample had a bulk density of  $1441 \text{ kg m}^{-3}$ , which lead to a density-derived vesicularity of 0.49. Image analysis of the control sample revealed a 2D vesicularity of 0.52 (Table 3). In contrast, quenched samples had lower densities (averaged at  $1161 \pm 171 \text{ kg m}^{-3}$ ) and therefore higher density-derived vesicularities (averaged at  $0.60 \pm 0.06$ ; Table 3). The difference in vesicularity between the control sample

**Table 2**

Chemical composition of the 61G lava flow (bulk rock from sample R12) and average of the interstitial glass composition (average of 10 to 15 analyses per sample; numbers in parentheses are the standard deviations).

	Bulk rock (wt.%)	Glass (wt.%)
SiO <sub>2</sub>	50.82	51.95 (0.09)
TiO <sub>2</sub>	2.45	2.77 (0.03)
Al <sub>2</sub> O <sub>3</sub>	13.71	13.33 (0.05)
FeO <sup>a</sup>	11.18	11.84 (0.18)
MnO	0.18	0.18 (0.01)
MgO	6.91	6.27 (0.1)
CaO	11.41	10.73 (0.08)
Na <sub>2</sub> O	2.43	2.42 (0.03)
K <sub>2</sub> O	0.62	0.50 (0.01)
P <sub>2</sub> O <sub>5</sub>	0.24	0.03 (0.01)
Cr <sub>2</sub> O <sub>3</sub>	—	0.02 (0.01)
H <sub>2</sub> O <sup>tot</sup>	—	0.077 (0.015)
LOI	−0.68	—
Total	99.36	100
Mg #	0.38	0.35

Bulk rock oxide composition is normalized to a total of 100% but measured total is also reported.

LOI: Loss of Ignition.

H<sub>2</sub>O<sub>tot</sub> measure by FTIR see supplementary material.

<sup>a</sup> Total iron is presented as FeO.

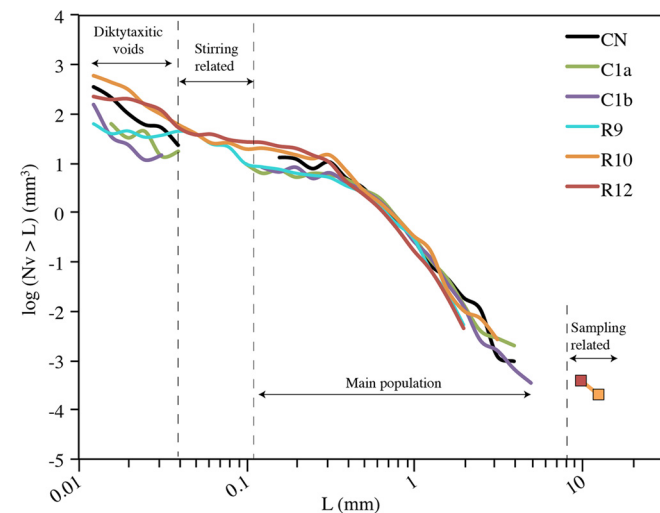


**Fig. 5.** The cumulative vesicle number density plot considers the vesicle number density per volume in mm<sup>−3</sup> ( $N_v$ ) with diameter greater than  $L$  (the equivalent diameter in mm) for all samples. C1a and C1b are both from sample C1 but from thin sections made perpendicular to each other. The orange and red squares represent the large vesicles related to the injection of air during sampling for R10 and R12, respectively.

**Table 3**

Textural analyses of the samples. Bulk density is the density of clasts measured with the Geopyc; density-derived vesicularity is obtained from bulk density and DRE density of 2847 kg m<sup>−3</sup>. Standard deviations are based on two-to-four measurements per samples and are given in parentheses.  $\phi_v$  = fraction of vesicles (2D vesicularity); Ol + Px vol.% = percentage of olivine + pyroxene;  $R_{ol+px}$  = aspect ratio of olivine + pyroxene; Plg vol.% = percentage of plagioclase;  $R_{plg}$  = aspect ratio of plagioclase;  $\phi_{xtl}$  = vesicle-free crystal (phenocrysts + microlites) fraction.

Sample	Bulk density (kg m <sup>−3</sup> )	Density-derived vesicularity $\phi$	$\phi_v$	Ol + Px (vol.%)	$R_{ol+px}$	Plg (vol.%)	$R_{plg}$	$\phi_{xtl}$
CN	1441 (0.03)	49.37 (0.96)	0.52	3.6	1.7	6.7	2.8	0.21
C1a	1030 (0.17)	63.87 (6.15)	0.53	3	1.9	2.8	3	0.12
C1b	960 (0.02)	66.18 (0.53)	0.49	2.7	1.7	3.2	3.3	0.12
R9	1294 (0.18)	54.52 (6.22)	0.42	6.3	1.8	5.4	3.3	0.20
R10	1096 (0.12)	61.49 (4.21)	0.57	2.3	2	3.4	3.2	0.13
R12	1145 (0.04)	59.75 (1.27)	0.44	3.6	1.7	4.7	2.9	0.15

and the quenched samples was due to the presence of isolated vesicles larger than 8 mm in the latter (see R12 in Fig. 4). Although not always observed in thin section, these large vesicles were always present in the quenched samples (as observed in hand specimen and as inferred from the higher density-derived vesicularity). The formation of these large vesicles was likely due to the ingestion of air in the molten lava during sampling, either when the tube was inserted or when the vane was withdrawn. To evaluate the bubble fraction in the flowing lava and during viscosity measurements, the vesicularity of the quenched samples therefore needed to be corrected for these large vesicles that represent artifacts introduced by the sampling process. Vesicle size distributions revealed that, for all the samples, there was a common population of spherical (when single) to convoluted (when two or more bubbles had coalesced) vesicles that range between 0.1 and 5 mm in size (Fig. 5). The average vesicle fraction obtained from the images (Table 3), which is that used here to estimate the effect of bubbles on viscosity, was  $0.50 \pm 0.06$ . All samples also contained a population of irregular micro-vesicles smaller than 0.03 mm. These were probably diktytaxitic voids related to the crystallization of microlites. We note that samples quenched after the viscosity measurement (R9, R10 and R12) also had a vesicle population between 0.03 to 0.1 mm that was not observed in either the control sample or the quenched sample from the sampling tube (Fig. 5). This population may have formed because of shearing during viscometry that led to disruption of larger bubbles to form smaller bubbles (Stein and Spera, 1992).

#### 4. Comparison with viscosity estimated from other techniques

##### 4.1. Petrologic approach using textural and chemical analyses

The parameters used for viscosity estimations via the petrologic approach are given in Table 4. Using the glass composition, and including the H<sub>2</sub>O content (Table 2) and the measured temperature (1144 °C), the viscosity of the melt phase was calculated using the model of Giordano et al. (2008) to be 330 Pa s. Note that a variation of  $\pm 1$  °C affected the melt viscosity by 2%. Considering the average vesicle-free crystal fraction, the mixture (melt + crystals) viscosity was estimated via the method described by Mader et al. (2013) for rough particles with an aspect ratio of 2.4, this being the average value calculated for all the crystals. The resulting bubble-free mixture viscosity is 699 Pa s. Note that a variation of  $\pm 1$  vol.% in crystallinity changed the viscosity by 6%. The effect of bubbles on the mixture viscosity depends on their ability to deform. We calculated the bubble capillary number ( $Ca$ ) from the applied shear rates during the viscosity measurements ( $3.5 \text{ s}^{-1}$  on average), with a modal bubble radius of 0.34 mm. Using the melt viscosity as calculated above and a bubble–liquid interfacial tension of  $0.3 \text{ N m}^{-1}$  (Murase and McBirney, 1973), we obtained a  $Ca$  of 1.3. Following Llewellyn and Manga (2005), 50 vol.% of deformable bubbles would lower the viscosity by a factor of 0.31, to give a bulk viscosity of the three-phase mixture (melt + crystals + bubbles) of



**Table 4**

Rheological parameters estimated via the petrologic approach using the chemical and textural characteristics averaged for all samples, and for samples quenched after viscosity measurements (R9, R10 and R12).

		All samples	R9	R10	R12
<b>Melt viscosity</b>					
VFT parameters <sup>a</sup>	A	−4.55			
	B	5901.7			
	C	582.2			
Melt viscosity (Pa s) at 1144 °C <sup>a</sup>		330			
<b>Effect of crystal on viscosity</b>					
Mean crystal fraction <sup>b</sup>	$\phi_{xtl}$	0.16	0.19	0.14	0.13
Average crystal aspect ratio	R	2.4	2.6	2.6	2.3
Maximum packing <sup>c</sup>	$\phi_m$	0.51	0.50	0.50	0.52
Relative viscosity (effect of crystals) <sup>d</sup>		2.0	2.6	1.9	1.8
Melt + crystal viscosity (Pa s)		699	849	632	590
<b>Effect of bubbles on viscosity</b>					
Mean vesicle fraction	$\phi_v$	0.5	0.42	0.57	0.44
Mean vesicle radius		0.34	0.39	0.39	0.31
Relative viscosity (effect of bubbles) <sup>e</sup>		0.31	0.41	0.24	0.38
<b>Melt + crystal + bubble viscosity (Pa s)</b>		<b>220</b>	<b>345</b>	<b>155</b>	<b>225</b>

<sup>a</sup> Calculated using glass composition (Table 2) via Giordano et al. (2008).

<sup>b</sup> Bubble-free mixture considering phenocrysts and microphenocrysts.

<sup>c</sup> Calculated for rough particles according to Eq. (49) in Mader et al. (2013).

<sup>d</sup> Calculated via Maron-Pierce (1956).

<sup>e</sup> Calculated via Llewellyn and Manga (2005) for  $Ca > 1$ .

220 Pa s. Accounting for the variability in crystal ( $\pm 4$  vol.%), bubble ( $\pm 6$  vol.%) and water ( $\pm 0.015$  wt.%) content this value varied by  $\pm 130$  Pa s. Thus, when accounting for deformable bubbles, the petrologic model provided a reasonable approximation to the field-measured viscosity. In contrast, neglecting the effect of bubbles, or considering bubbles as non-deformable solid particles, would lead to a significant overestimation in viscosity (this being  $> 10^3$  Pa s). We note that the differences in viscometer-measured viscosity between each lobe did not exactly correlate with the model-based viscosity estimation made from the crystal and bubble content of the quenched samples (Fig. 3). This can either be explained by our field viscosity measurements needing better accuracy, or because the rheological models used in the petrologic approach were inappropriate.

#### 4.2. Laboratory results from previous studies

Laboratory viscometry of crystallizing Hawaiian lavas at subliquidus temperatures were performed by Shaw (1969), Ryerson et al. (1988), and Sehlke et al. (2014). The main difference between these experiments and field measurements is the absence of bubbles in the laboratory experiments. Another important difference is that crystallization in the laboratory always takes place at a higher temperature than in nature and, consequently, viscosity will always be greater at any given temperature in the laboratory experiments. This is mainly due to three reasons. First, laboratory experiments are usually performed under atmospheric conditions at 1 atm with an oxidized oxygen fugacity and a completely degassed melt. Second, constant stirring of the melt during viscosity measurement enhances crystallization (Kouchi et al., 1986; Vona and Romano, 2013; Chevrel et al., 2015). Third, most laboratory experiments apply isothermal conditions and are at thermodynamic equilibrium. This results in higher crystal contents than under steady cooling (disequilibrium) as in nature (Kolzenburg et al., 2016). For example, at 1144 °C (the lava temperature measured in the field), experiments by Sehlke et al. (2014) would predict a crystal content of almost 100% and a viscosity of more than  $10^5$  Pa s. Comparing the experiments of Shaw (1969) and Ryerson et al. (1988) at this same temperature, viscosity would be predicted to be almost the same as we measured but with a much higher crystal content [25 and  $> 45$  vol.% for Shaw (1969) and Ryerson et al. (1988), respectively].

Following Ryerson et al. (1988) the lava should have a yield strength of 28 Pa and 125 Pa for 15 and 25 vol.% crystals, respectively, while following Sehlke et al. (2014), the yield strength should be lower. However, whether a crystal content as low as 15 to 25 vol.% would build a crystal framework and develop a yield strength is a matter of ongoing debate (Saar et al., 2001). Any yield strength present during our experiments was smaller than the level of detectability of the instrument which means that – if present – the yield strength is less than 300 Pa. Lower strain rates and a more sensitive torque sensor are required to improve measurement sensitivity. Additionally, better constraints on estimating the yield strength from the petrologic approach and that considers crystals and bubbles are needed (see discussion in Chevrel et al., 2013; Castruccio et al., 2014).

#### 4.3. Previous field-based viscometry measurements

Two previous *in situ* field viscosity measurements were undertaken on Hawaiian lavas. The first measurements were made at Makaopuhi lava lake by Shaw et al. (1968) using a vertical rotational viscometer. They recorded a viscosity of 650–720 Pa s for a unit strain rate and yield strengths of 70 and 120 Pa. The collected samples and *in situ* temperature measurements revealed  $< 5\%$  vesicles and a crystallinity of 25% at  $1130 \pm 5$  °C. Although our samples had a higher silica content, our viscosity measurements were slightly lower. This is explained by a combination of lower crystal fraction, higher content of deformable bubbles and higher temperature. The other set of measurements was performed by Pinkerton et al. (1995b) on three 0.2 to 0.5 m thick pāhoehoe lobes erupted in September 1994 at Kilauea using the same rotational viscometer as used in this study but equipped with a more sensitive torque sensor. Maximum measured temperatures were 1146 °C and apparent viscosities at unit strain rate were in the range 234–548 Pa s. The lowest viscosity lobe was also the closest to Newtonian behavior and was best characterized by a power law model of the form  $\tau = 234\dot{\gamma}^{0.77}$ . The highest viscosity lobe departed significantly from Newtonian behavior and fitted a power law model with the form  $\tau = 548\dot{\gamma}^{0.53}$ . The non-Newtonian behavior measured in 1994 might reflect different vesicularities or crystallinities compared with those of the 2016 lavas, however samples collected in 1994 were not analyzed. Alternatively, it could be the result of operating the instrument at lower rotational speeds and

hence strain rates ( $<1 \text{ s}^{-1}$ ) in 1994. This permitted construction of a complete rheological curve (Fig. 3). Although some differences were observed between the 1994 and 2016 measurements, the results of both studies agreed on the range in apparent viscosities at unit strain rate (Fig. 3).

## 5. Discussion

We have compared our field viscosity measurements with estimations of lava viscosity from the petrologic approach and from previous laboratory and field measurements. However, the measured values represent only a “snap shot” of the lava interior behavior over a short time scale and at a single temperature. Indeed, pāhoehoe lobes cool very quickly (e.g., Hon et al., 1994; Ball et al., 2008; Gottsmann et al., 2004). Ball et al. (2008) showed that small stationary lobes (without advection of hot lava) and non-stationary lobes cool to  $800^\circ\text{C}$  in 25 s and 50 s, respectively. Thus, lobe cooling will lead to a rapid increase in viscosity that will quite quickly impede viscosity measurement. This was observed during our measurements when the vane became stuck or when viscosity measurements dramatically increased, sometimes after only 10 s. In general, we observed that viscosity always increased with time; which likely reflected the cooling effect of the whole lobe. The increase of viscosity with time, could also be due to accumulation of lava around the vane due to the chilling effect of the vane being inserted, which increased the apparent vane diameter. To discriminate between lobe cooling or accumulation effects, further field viscosity measurements need to be performed while continuously recording the temperature at the vane. For this, the rotating vane should be equipped with a thermocouple, as has been recently achieved in the laboratory (Kolzenburg et al., 2016). This type of measurement will allow tracking of the temperature, and therefore the cooling rate – viscosity relationship, which is a key to understanding the thermo-rheological control of lava flow emplacement (Giordano et al., 2007; Kolzenburg et al., 2017, 2016). Another problem that was faced during our measurements was the cooling of the lobe crust around the rotating shaft. Indeed, the lobe surface cooled more rapidly than its interior (Hon et al., 1994), which may lead to friction around the rotating shaft and disturbed the measurements. Future instrument refinement is required to protect the shaft from the outer cooling crust.

The results presented here, including the integration of viscosity field measurement and detailed textural analyses, are a first step toward quantifying the behavior of lava whilst accounting for all its components (melt, crystals and bubbles). Indeed, a major advantage of field measurements compared with those made in the laboratory is their ability to measure the behavior of a three-phase mixture of lava in its natural and original state. One of the difficulties in laboratory experiments is that sample preparation (i.e., melting the lava in the laboratory) leads to degassing and loss of volatiles, making accurate measurement of lava containing bubbles challenging, if not impossible. Direct comparisons between the laboratory experiments and measurements made in the field are therefore difficult for now. Recreating field conditions in the laboratory (in particular volatile content, oxygen fugacity, cooling rate and shear rate) is an ongoing challenge and a goal for future experiments (Kolzenburg et al., 2017). Therefore, field measurement using a rotating viscometer offers a promising solution to quantifying three-phase lava viscosity relations at high temperature. Future field viscometry holds the potential to evaluate the effects of three-phase mixtures on rheology, in particular the role of bubbles, and bubble-bubble or bubble-crystal interactions, over a large range of strain rate.

For this, future field viscometers need to be more versatile so as to measure small torques at low applied strain rates. This will allow the complete flow curve to be recorded (Pinkerton et al.,

1995b). Future instruments also need to be lighter so that one operator can carry out rapid measurements from a vent to a flow front, and in very remote places. Such measurements can be envisaged on well-channelized narrow flows with stable levées or at breakouts at various distances from the vent (e.g., Belousov and Belousova, 2018). With associated sample analyses and synchronous temperature measurement, field viscometry will be sufficiently precise to record the temperature- and time-dependent rheological transformations of lava and provide a benchmark for calibrating lava flow emplacement models. Measurements on various lava compositions, temperatures, and/or crystal and bubble content will also lead to improved quantification of lava rheology.

## 6. Conclusions

Viscosity measurements performed in the field by introducing a rotational viscometer directly into flowing lava, along with simultaneous sampling to allow the associated textural and chemical characteristics to be defined, were non-existent. We successfully measured the viscosity of several lobes that had an average of 380 Pa s for strain-rates between 1.6 and  $5 \text{ s}^{-1}$  and a temperature of  $1144^\circ\text{C}$ . Although the full rheological curves could not be measured due to instrumental limitations and challenging field conditions, this result is in agreement with previous studies and confirms the range of apparent viscosities at unit strain rate for Hawaiian lavas. In contrast to previous studies, our measurements were made alongside simultaneous collection of quenched lava samples, which we thoroughly analyzed by quantifying the chemical and textural characteristics. This provides a unique benchmark allowing field-based, laboratory-based and theoretical models to be compared and their accuracy, error and uncertainty to, for the first time, be assessed. Comparison of our measurements with viscosity estimated from a petrologic approach or from previous field and laboratory studies shows that the petrologic approach, when carried out with rigorous textural analyses of the collected samples, provides viscosity estimates that are in approximate agreement with field measurements. Quantification of the effect of crystals and bubbles is, however, extremely important if we are to correctly apply a model. Isothermal laboratory measurements prove to be the most precise method in describing the full flow curve, but cannot be applied directly to natural flows as crystallization takes place at higher temperatures and they cannot account for the effect of bubbles. We thus find that dynamic cooling experiments in conjunction with field measurements are needed to fully understand the lava emplacement rheology. Field viscometry accompanied by thorough analyses of quenched samples is the most promising approach to quantify evolving lava rheology in time and space. Collecting several measurements down a single flow system or at several flow units with different characteristics (temperature of effusion, cooling rate, composition, crystal and bubble content) will lead to proper benchmarking for lava flow modeling.

## Acknowledgements

This research was financed by the French Government Laboratory of Excellence initiative No. ANR-10-LABX-0006, the Region Auvergne and the European Regional Development Fund. MOC acknowledges the Auvergne fellowship for full support and the Cler-Volc program 6 for field support. This is Laboratory of Excellence ClerVolc contribution No. 296. The authors gratefully acknowledge Matthew Patrick, the Hawaiian Volcano Observatory and Hawaiian Volcanoes National Park where work was completed under National park permit HAVO-2016-SCI-0064. The pole technique of LMV, including Jean-Louis Fruquière, Cyrille Guillot, Christophe Constantin, Jean-Luc Devidal, Jean-Marc Henot and Federica Schiavi, is acknowledged for instrument modifications, sample prepa-

ration and sample analyses. Field measurements were performed with the help of Alejandra Gomez-Ulla, Guillem Pinto-Gisbert, Matthew Burgess and Matthew Patrick who are greatly acknowledged. Additionally, Antonio Caponi, Alejandra Gomez-Ulla, Marie-Anne Ancelin, Valentin Gueugneau and Romina Severino are acknowledged for lab assistance during instrument calibration. Finally, Tamsin Mather (editor), Stephan Kolzenburg and Alessandro Vona (reviewers) are gratefully acknowledged for their thorough reviews and suggestions, which significantly improved the message of this contribution.

## Appendix A. Supplementary material

Supplementary material related to this article can be found online at <https://doi.org/10.1016/j.epsl.2018.04.028>.

## References

- Applegarth, L.J., Tuffen, H., James, M.R., Pinkerton, H., 2013. Degassing-driven crystallisation in basalts. *Earth-Sci. Rev.* 116, 1–16.
- Ball, M., Pinkerton, H., Harris, A.J.L., 2008. Surface cooling, advection and the development of different surface textures on active lavas on Kilauea, Hawai'i. *J. Volcanol. Geotherm. Res.* 173 (1–2), 148–156.
- Barnes, H.A., Hutton, J.F., Walters, K., 1989. *An Introduction to Rheology*. Rheology Series, vol. 3. Elsevier Science, U.S. and Canada.
- Belousova, A., Belousova, M., 2018. Dynamics and viscosity of 'a'ā and pāhoehoe lava flows of the 2012–2013 eruption of Tolbachik volcano, Kamchatka (Russia). *Bull. Volcanol.* 80 (6).
- Castruccio, A., Rust, A.C., Sparks, R.S.J., 2014. Assessing lava flow evolution from post-eruption field data using Herschel–Bulkley rheology. *J. Volcanol. Geotherm. Res.* 275, 71–84.
- Chevrel, M.O., Cimarelli, C., DeBiasi, L., Hanson, J.B., Lavallée, Y., Arzilli, F., Dingwell, D.B., 2015. Viscosity measurements of crystallizing andesite from Tungurahua Volcano (Ecuador). *Geochim. Geophys. Geosyst.* 16 (3).
- Chevrel, M.O., Platz, T., Hauber, E., Baratoux, D., Lavallée, Y., Dingwell, D.B., 2013. Lava flow rheology: a comparison of morphological and petrological methods. *Earth Planet. Sci. Lett.* 384, 102–120.
- Cordonnier, B., Lev, E., Garel, F., 2015. Benchmarking lava-flow models. In: Harris, A.J.L., De Groeve, T., Garel, F., Carn, S.A. (Eds.), *Detecting, Modelling and Responding to Effusive Eruptions*. In: *Geol. Soc. (Lond.) Spec. Publ.*, vol. 426.
- Crisp, J., Cashman, K.V., Bonini, J.A., Houghton, S.B., Pieri, D.C., 1994. Crystallization history of the 1984 Mauna Loa lava flow. *J. Geophys. Res.* 99 (B4), 7177–7198.
- Dingwell, D.B., 1996. Volcanic dilemma flow or blow. *Science* 273, 1054–1055.
- Einarsson, T., 1949. The flowing lava. *Studies of its main physical and chemical properties*. In: *The Eruption of Hekla 1947–1948, IV. Soc. Scientiarum Islandica, Reykjavik*, pp. 1–70.
- Gauthier, F., 1973. Field and laboratory studies of the rheology of Mount Etna Lava. *Philos. Trans. R. Soc. Lond. A, Math. Phys. Eng. Sci.* 274 (1238), 83–98.
- Giordano, D., Polacci, M., Longo, A., Papale, P., Dingwell, D.B., Boschi, E., Kasereka, M., 2007. Thermo-rheological magma control on the impact of highly fluid lava flows at Mt. Nyiragongo. *Geophys. Res. Lett.* 34 (L06301).
- Giordano, D., Russell, J.K., Dingwell, D.B., 2008. Viscosity of magmatic liquids: a model. *Earth Planet. Sci. Lett.* 271 (1–4), 123–134.
- Gottsmann, Joachim, Harris, Andrew J.L., Dingwell, Donald B., 2004. Thermal history of Hawaiian pāhoehoe lava crusts at the glass transition: implications for flow rheology and emplacement. *Earth Planet. Sci. Lett.* 228 (3–4), 343–353.
- Harris, A.J.L., Rowland, S.K., 2001. FLOWGO: a kinematic thermo-rheological model for lava flowing in a channel. *Bull. Volcanol.* 63, 20–44.
- Hon, K., Kauahikaua, J., Denlinger, R., Mackay, K., 1994. Emplacement and inflation of pāhoehoe sheet flows: observations and measurements of active lava flows on Kilauea Volcano, Hawaii. *Geol. Soc. Am. Bull.* 106, 351–370.
- Houghton, B.F., Wilson, C.J.N., 1989. A vesicularity index for pyroclastic deposits. *Bull. Volcanol.* 51 (6), 451–462.
- Ishibashi, H., 2009. Non-Newtonian behavior of plagioclase-bearing basaltic magma: subliquidus viscosity measurement of the 1707 Basalt of Fuji Volcano, Japan. *J. Volcanol. Geotherm. Res.* 181, 78–88.
- James, M.R., Pinkerton, H., Robson, S., 2007. Image-based measurement of flux variation in distal regions of active lava flows. *Geochim. Geophys. Geosyst.* 8 (3).
- Kolzenburg, S., Giordano, D., Cimarelli, S., Dingwell, D.B., 2016. In situ thermal characterization of cooling/crystallizing lavas during rheology measurements and implications for lava flow emplacement. *Geochim. Cosmochim. Acta* 195, 244–258.
- Kolzenburg, S., Giordano, D., Thordarson, T., Hoskuldsson, A., Dingwell, D.B., 2017. The rheological evolution of the 2014/2015 eruption at Holuhraun, Central Iceland. *Bull. Volcanol.* 79 (45).
- Kouchi, Akira, Tsuchiyama, Akira, Sunagawa, Ichiro, 1986. Effect of stirring on crystallization kinetics of basalt: texture and element partitioning. *Contrib. Mineral. Petrol.* 93 (4), 429–438.
- Llewellyn, E.W., Manga, M., 2005. Bubble suspension rheology and implications for conduit flow. *J. Volcanol. Geotherm. Res.* 143, 205–217.
- Mader, H.M., Llewellyn, E.W., Mueller, S.P., 2013. The rheology of two-phase magmas: a review and analysis. *Bull. Volcanol.* 257, 135–158.
- Mercier, M., Di Muro, A., Metrich, N., Giordano, D., Belhadj, O., Mandeville, C.W., 2010. Spectroscopic analysis (FTIR, Raman) of water in mafic and intermediate glasses and glass inclusions. *Geochim. Cosmochim. Acta* 74, 5641–5656.
- Moore, H.J., 1987. Preliminary estimates of the rheological properties of 1984 Mauna Loa Lava. In: *U.S. Geological Survey Professional Paper*, vol. 1350, pp. 1569–1588.
- Murase, T., McBirney, A.R., 1973. Properties of some common igneous rocks and their melts at high temperatures. *Geol. Soc. Am. Bull.* 84, 3563–3592.
- Nichols, R.L., 1939. Viscosity of lava. *J. Geol.* 47 (3), 290–302.
- Panov, V.K., Slezin, Yu.B., Storcheus, A.V., 1988. Mechanical properties of lavas extruded in the 1983 Predskazannyi eruption (Klyuchevskoy Volcano). *Volcanol. Seismol.* 7, 25–37.
- Pinkerton, H., 1994. Rheological and related properties of lavas. In: Dobran, F. (Ed.), *Etna: Magma and Lava Flow Modeling and Volcanic System Definition Aimed at Hazard Assessment*. Global Volcanic and Environmental System Simulation, pp. 76–89.
- Pinkerton, H., Norton, G., 1995. Rheological properties of basaltic lavas at sub-liquidus temperatures: laboratory and field measurements on lavas from Mount Etna. *J. Volcanol. Geotherm. Res.* 68, 307–323.
- Pinkerton, H., Sparks, R.S.J., 1978. Field measurements of the rheology of lava. *Nature* 276, 383–385.
- Pinkerton, H., Stevenson, R.J., 1992. Methods of determining the rheological properties of magmas at sub-liquidus temperatures. *J. Volcanol. Geotherm. Res.* 53, 47–66.
- Pinkerton, H., Herd, R.A., Kent, R.M., Wilson, L., 1995a. Field measurements of the rheological properties of basaltic lavas. *Lunar Planet. Sci. XXVI*, 1127–1128.
- Pinkerton, H., Norton, G.E., Dawson, J.B., Pyle, D.M., 1995b. Field observations and measurements of the physical properties of Oldoinyo Lengai alkali carbonate lavas, November 1988. In: Bell, K., Keller, J. (Eds.), *IAVCEI Proceedings in Volcanology 4: Carbonatite Volcanism of Oldoinyo Lengai – Petrogenesis of Natro-carbonatite*. Springer-Verlag, Berlin, pp. 23–36.
- Riker, J.M., Cashman, K.V., Kauahikaua, J.P., Montierth, C.M., 2009. The length of channelised lava flows: insight from the 1859 eruption of Mauna Loa Volcano, Hawaii. *J. Volcanol. Geotherm. Res.* 183, 139–156.
- Robert, B., Harris, A., Gurioli, G., Medard, E., Sehlke, A., Whittington, A., 2014. Textural and rheological evolution of basalt flowing down a lava channel. *Bull. Volcanol.* 76, 824.
- Ryerson, F.J., Weed, H.C., Piwinski, A.J., 1988. Rheology of subliquidus magmas: picritic compositions. *J. Geophys. Res.* 93, 3421–3436.
- Saar, M.O., Manga, M., Cashman, K.V., Fremouw, S., 2001. Numerical models of the onset of yield strength in crystal-melt suspensions. *Earth Planet. Sci. Lett.* 187 (3–4), 367–379.
- Sehlke, A., Whittington, A., Robert, B., Harris, A.J.L., Gurioli, L., Médard, E., 2014. Pāhoehoe to 'a'ā transition of Hawaiian lavas: an experimental study. *Bull. Volcanol.* 76, 876.
- Shaw, H.R., 1969. Rheology of basalt in the melting range. *J. Petrol.* 10, 510–535.
- Shaw, H.R., Wright, T.L., Peck, D.L., Okamura, R., 1968. The viscosity of basaltic magma: an analysis of field measurements in Makaopuhi Lava Lake, Hawaii. *Am. J. Sci.* 266, 225–264.
- Shea, T., Houghton, B.F., Gurioli, L., Cashman, K.V., Hammer, J.E., Hobden, B.J., 2010. Textural studies of vesicles in volcanic rocks: an integrated methodology. *J. Volcanol. Geotherm. Res.* 190 (3–4), 271–289.
- Spera, F.J., Borgia, A., Strimple, J., Feigenson, M., 1988. Rheology of melts and magmatic suspensions. I: design and calibration of a concentric cylinder viscometer with application to rhyolitic magma. *J. Geophys. Res.* 93, 10273–10294.
- Stein, D.J., Spera, F.J., 1992. Rheology and microstructure of magmatic emulsions: theory and experiments. *J. Volcanol. Geotherm. Res.* 49, 157–174.
- Stein, D.J., Spera, F.J., 1998. New high-temperature rotational rheometer for silicate melts, magmatic suspensions, and emulsions. *Rev. Sci. Instrum.* 69, 3398–3402.
- Vetere, F., Sato, H., Ishibashi, H., De Rosa, R., Donato, P., Ishibashi, H., De Rosa, R., Donato, P., 2013. Viscosity changes during crystallization of a shoshonitic magma: new insights on lava flow emplacement. *J. Mineral. Petrol. Sci.* 108 (3), 144–160.
- Vona, A., Romano, C., 2013. The effects of undercooling and deformation rates on the crystallization kinetics of Stromboli and Etna Basalts. *Contrib. Mineral. Petrol.* 166 (2), 491–509.
- Vona, A., Romano, C., Dingwell, D.B., Giordano, D., 2011. The rheology of crystal-bearing basaltic magmas from Stromboli and Etna. *Geochim. Cosmochim. Acta* 75, 3214–3236.